


Structural study of some unsaturated malononitriles using mass spectrometry and theoretical models

Federico M. Garófalo^{1,2} | Belén Gastaca^{2,3} | Alberto Albesa^{2,4} |
Jorge J. P. Furlong^{1,2} | Patricia E. Allegretti^{1,2} | Juan M. Giussi² 

¹Centro de Estudio de Compuestos Orgánicos (CEDECOR) - Facultad de Ciencias Exactas, Universidad Nacional de La Plata, La Plata, Argentina

²Facultad de Ciencias Exactas, Universidad Nacional de La Plata (1900), La Plata, Argentina

³Laboratorio UPL, CIC - Universidad Nacional de La Plata, La Plata, Argentina

⁴Instituto de Investigaciones Fisicoquímicas Teóricas y Aplicadas (INIFTA), CCT-La Plata - Universidad Nacional de La Plata, La Plata, Argentina

Correspondence

Juan M. Giussi, Facultad de Ciencias Exactas, Universidad Nacional de La Plata (1900), La Plata, Argentina.
Email: jmgussi@quimica.unlp.edu.ar

Abstract

The study of tautomerism has gained relevance in the scientific community because several cellular processes occur through different tautomeric forms of certain compounds. The percentage of each tautomer in compounds with tautomerism capability depends on numerous factors, such as temperature and solvent polarity, among others; and, by changing the external conditions, equilibrium displacement can be established very quickly. This manuscript deals with nitrile–ketenimine tautomerism in some unsaturated malononitriles. This kind of compounds with two nitrile groups conjugated to a double bond is able to rearrange accessible hydrogens and provide new and complex structures of different functionalities. The authors' motivation for investigating these compounds lies in understanding their tautomeric behavior in solution and gas phases and to predict reaction department to then account for the final products obtained. Four unsaturated malononitriles were synthesized to study the substituent effect on equilibrium displacement. Characterization was performed using nuclear magnetic resonance (NMR) and tautomeric equilibrium in gas phase was evaluated by mass spectrometry. Correlation with theoretical calculations was carried out in order to comprehend the system behavior.

KEYWORDS

DFT calculations, nitrile–ketenimine tautomerism, NMR and mass spectrometry, unsaturated malononitriles

1 | INTRODUCTION

Numerous cellular processes occur through tautomeric forms of compounds that potentially have tautomerizable groups, and a variety of reactions can be controlled through the displacement of this type of equilibrium.^{1–5} Singh et al.⁶ described that tautomeric nucleoside analogs can act as antiviral drugs due to their ability to induce lethal mutagenesis. After many viruses, such as human immunodeficiency virus (HIV) and COVID-19,

infect a cell, they rapidly begin making copies of their genetic material. Lethal mutagenesis is a novel therapeutic strategy that exploits the high mutation rates of certain viruses by intentionally increasing the viral mutation rate, causing excessive error accumulation and causing the viral population to collapse.⁷

From a chemical viewpoint, the study of the tautomeric equilibrium in compounds with the ability to tautomerize is determined by the stability of the different tautomers.^{8,9} Several works in the literature use

mass spectrometry to elucidate structural aspects of functional groups, but few deal with how this technique can be applied to different types of tautomerism.^{10,11}

Of the many functional groups useful in organic synthesis, the cyano group is one of the most versatile.^{12,13} The literature on the biochemistry of the cyano group has revealed the central role of nitriles in plant biochemistry.¹⁴ For instance, cyanogenesis (HCN formation) is one of the simplest forms of plant taxonomy. In fact, many species have been classified based on their HCN production.^{15,16} Cyano compounds with one or more hydrogens bonded to the alpha carbon are potentially capable of exhibiting nitrile–ketenimine tautomerism (Scheme 1A). If two hydrogens are contained on the alpha carbon, the presence of an inamine structure can be also expected (Scheme 1B).

Strongly electron-attracting substituents on the alpha carbon were noticed to shift the equilibrium toward the ketenimine form.¹⁷ Few works have reported the occurrence of nitriles in equilibrium with their corresponding ketenimine tautomer. Nonetheless, some of them have concluded that, to a certain extent, equilibrium occurs.^{18–20} Using ab initio calculations, Sung et al.²¹ concluded that the amination of cetenimines proceeds via addition to the C=N double bond rather than to the C=C double bond and this results to a variety of reactions that can be controlled through the displacement of this type of equilibrium.

Because malononitrile are acid compounds that can be used as a nucleophile in a wide variety of reactions in organic chemistry,^{22–24} the aim of this work was to study experimentally the tautomerism in gas phase of some unsaturated malononitriles by mass spectrometry and to correlate the results with a theoretical model. The analysis of these simple structures further allowed to correlate their reactivity with the chemical behavior of complex systems, such as biomolecules.

2 | EXPERIMENTAL

2.1 | Materials

Malononitrile (99%), 4-phenylbutan-2-one (99%), 1-phenylpropan-2-one (99%), phenylmethyl ketone (99%), benzaldehyde (99%), ammonium acetate (99%), acetic acid (99%), benzene (99%), sodium bicarbonate (99%), and sodium sulfate (99%) were obtained from Sigma-Aldrich.

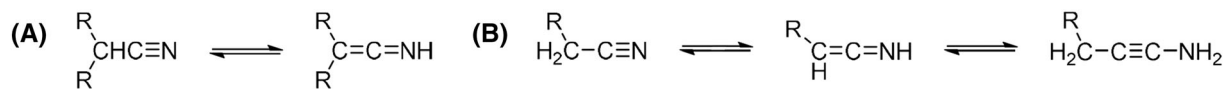
2.2 | Synthesis

Four malononitriles with different substituents were obtained through an adaptation of a method previously described.¹² The general synthesis reaction is described below (Scheme 2), along with the procedure for each compound.

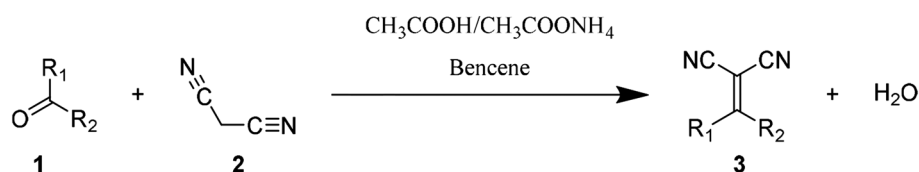
2.2.1 | 2-(4-Phenylbutan-2-ylidene) malononitrile (FBIM)

In a 250-mL round-bottom flask, 15.4 g of 4-phenylbutan-2-one, 7.05 g of malononitrile, 1.4 g of ammonium acetate, 3.5 mL of acetic acid, and 52.5 mL of benzene were mixed. A Dean Stark trap and a condenser were coupled, and the reaction was carried out for 2.5 h at reflux with magnetic stirring. The end point of the reaction was determined by thin layer chromatography (TLC) at which time the trap contained 1.55 mL of water.

The reaction product was washed with sodium bicarbonate solution (15%wt) and distilled water. The organic extract was dried with sodium sulfate and filtered off. The mixture was concentrated in a rotary evaporator until constant weight. The product was purified by distillation under vacuum (5 Torr) at 169–170°C. The reaction



SCHEME 1 (A) Nitrile–ketenimine tautomerism and (B) nitrile–ketenimine–inamine tautomeric equilibrium.



SCHEME 2 General synthetic method for selected unsaturated malononitriles. R₁ and R₂ substituents are specified below. (1) Carbonyl reagent, (2) malononitrile, and (3) unsaturated malononitrile.

yield was 68.3%. The product was identified by $^1\text{H-NMR}$, $^{13}\text{C-NMR}$, and gas chromatography–mass spectrometry (GC-MS). Spectra did not show impurity signals.

2.2.2 | 2-(1-Phenylpropan-2-ylidene) malononitrile (FPIM)

In a 250-mL round-bottom flask, 8.6 g of 1-phenylpropan-2-one, 4.3 g of malononitrile, 0.86 g of ammonium acetate, 2.15 mL of acetic acid, and 50 mL of benzene (recovered) were mixed. The mixture was reacted for 2 h under reflux with magnetic stirring. The end point of the reaction was terminated by TLC at which point the Dean Stark trap contained 1 mL of water.

The reaction product was washed with sodium bicarbonate solution (15%wt) and distilled water. The organic extract was dried with sodium sulfate and filtered off. The mixture was concentrated in a rotary evaporator until constant weight.

The concentrated product was purified by distillation under vacuum (5 Torr), obtaining a small fraction at 80°C (discarded) and a main fraction at 110°C as a colorless liquid. The reaction yield was 77%. The product was identified by $^1\text{H-NMR}$, $^{13}\text{C-NMR}$, and GC-MS. Spectra did not show impurity signals.

2.2.3 | 2-1(Phenylidene) malononitrile (FIM)

In a 250-mL round-bottom flask, 18 g of phenylmethyl ketone, 10 g of malononitrile, 5 mL of acetic acid, 2 g of ammonium acetate, and 75 mL of recovered benzene were mixed. The mixture was reacted for 2 h under reflux with magnetic stirring. The end point of the reaction was determined with TLC at which point the Dean Stark trap contained 2.2 mL of water and a homogeneous yellow solution was obtained. The reaction product was washed with sodium bicarbonate (15%wt) solution and water. The organic extract was dried with sodium sulfate and filtered off. The mixture was concentrated in a rotary evaporator to constant weight. The product was purified by distillation under vacuum (5 Torr), obtaining a small fraction at 65°C and a main fraction at 87°C as a colorless liquid that crystallized in the fridge. The reaction yield was 58%. The product was identified by $^1\text{H-NMR}$, $^{13}\text{C-NMR}$, and GC-MS. Spectra did not show impurity signals.

2.2.4 | 2-Benzylidenemalononitrile (BIM)

In a 250-mL round-bottom flask, 15.5 mL of benzaldehyde, 10 g of malononitrile, 5 mL of acetic acid, 2 g of

ammonium acetate, and 75 mL of recovered benzene were mixed. The mixture was reacted under reflux with magnetic stirring for 2 h. The end point of the reaction was determined with TLC at which point the Dean Stark trap contained 2 mL of water. A heterogeneous mixture containing two phases was obtained, a solid (brown) and a liquid (grayish yellow) one. The solid product, isolated by filtration, was purified by distillation under vacuum (5 Torr), obtaining a small first fraction at 60°C and a main fraction at 77°C as a colorless liquid. The reaction yield was 69%. The product was identified by $^1\text{H-NMR}$, $^{13}\text{C-NMR}$, and GC-MS. Spectra did not show impurity signals.

2.3 | Structural determinations

2.3.1 | ^1H NMR spectrometry

The ^1H NMR spectra of the studied compound were registered with a Varian Mercury Plus Spectrometer, 200 MHz. Chloroform- d_1 was used as solvent. The typical spectral conditions were as follows: spectral width 3201 Hz, acquisition time 4.09 s, and 8–16 scans per spectrum. Digital resolution was 0.39 Hz per point. Deuterated solvents were used, and tetramethylsilane was the internal standard. The sample concentration was 0.41 wt%, and the spectra were recorded at room temperature.

2.3.2 | Mass spectrometry

GC-MS of the compounds was performed by injecting methanol solutions (1 μL) in an HP 5890 Chromatograph (column HP5-MS, 30 m \times 0.25 mm \times 5 μm and helium as carrier gas at 0.6 mL/min) coupled to an HP 5972 A mass selective detector. Temperature set points as follows: injector: 250°C; oven: 40°C during the first 5 min and 20°C/min to 290°C; interface: 300°C; ion source: 185°C; and quadrupole: 150°C. Electron energy was set to 70 eV. Pressure in the mass spectrometer was set to 10^{-5} Torr.

2.3.3 | Computational methods

With the aim of correlating the experimental results and supporting the trends and observations found, geometry optimization calculations were performed using a DFT theory with the hybrid functional B3LYP and the set of bases 6-311 ++ g (d, p), as implemented in the ORCA package, all geometry optimizations were performed without restrictions.

2.4 | Isotopic exchange experiments

For each isotopic exchange experiment, 10 mg of each compound was mixed with 1 mL of deuterated methanol and 5 μ L of triethylamine. After 1 h at room temperature, the solutions were injected in a GC-MS.

3 | RESULTS AND DISCUSSION

The condensation between selected carbonyl compounds and malononitrile produced α - β unsaturated malononitrile whose structure and ^1H NMR assignments are provided in Table 1.

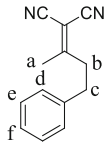
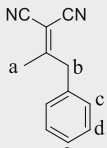
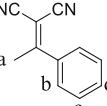
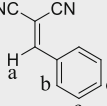
The isotopic exchange experiments were carried out as described in the experimental part and analyzed using GC-MS.

Regarding the undeuterated compounds, after purification, a single peak was observed in the chromatogram in all cases, and the mass spectra of the mentioned peaks confirmed the compounds in question: BIM, FIM, FPIM, and FBIM (Figures 1, 2A, 3A, and 4A, respectively).

After deuteration, in the case of BIM and FIM, only one peak was observed in the chromatograms. The MS of the BIM peak was the same as that of the starting compound (Figure 1), and the MS of the FIM peak was that corresponding to the deuterated product (Figure 2B). Interestingly, regarding FPIM and FBIM, two peaks were observed in the chromatogram spectrum, one corresponding to the deuterated products (Figures 3B and 4B, respectively) and the other to the dimeric ones (Figures 3C and 4C).

Figure 1 depicts the mass spectrum of BIM. Figure S1 shows the corresponding chromatogram, and Scheme 1

TABLE 1 Unsaturated malononitrile obtained with H NMR assignments.

Compound	Structure	H NMR signals in chloroform- d_1
2-(4-Phenylbutan-2-ylidene) malononitrile (FBIM)		(a) 1.81 ppm (s), 3H (b + c) 2.76 ppm (m), 4H (d + e + f) 7.1–7.4 ppm (m), 5H
2-(1-Phenylpropan-2-ylidene) malononitrile (FPIM)		(a) 1.85 ppm (s), 3H (b) 2.85 ppm (s), 2H (d + e + f) 7.0–7.4 ppm (m), 5H
2-1(Phenylidene) malononitrile (FIM)		(a) 2.03 ppm (s), 3H (b + c + d) 6.9–7.3 ppm (m), 5H
2-Benzylidenemalononitrile (BIM)		(a) 7.88 ppm (s), 1H (b + c + d) 6.8–7.4 ppm (m), 5H

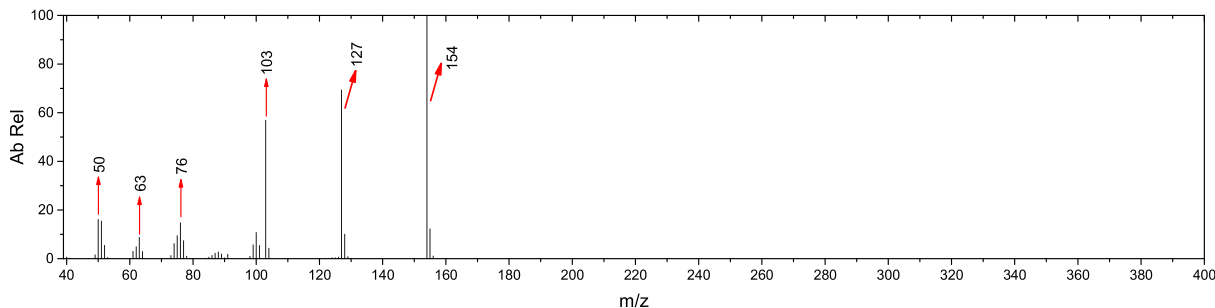


FIGURE 1 Mass spectrum of 2-benzylidenemalononitrile.

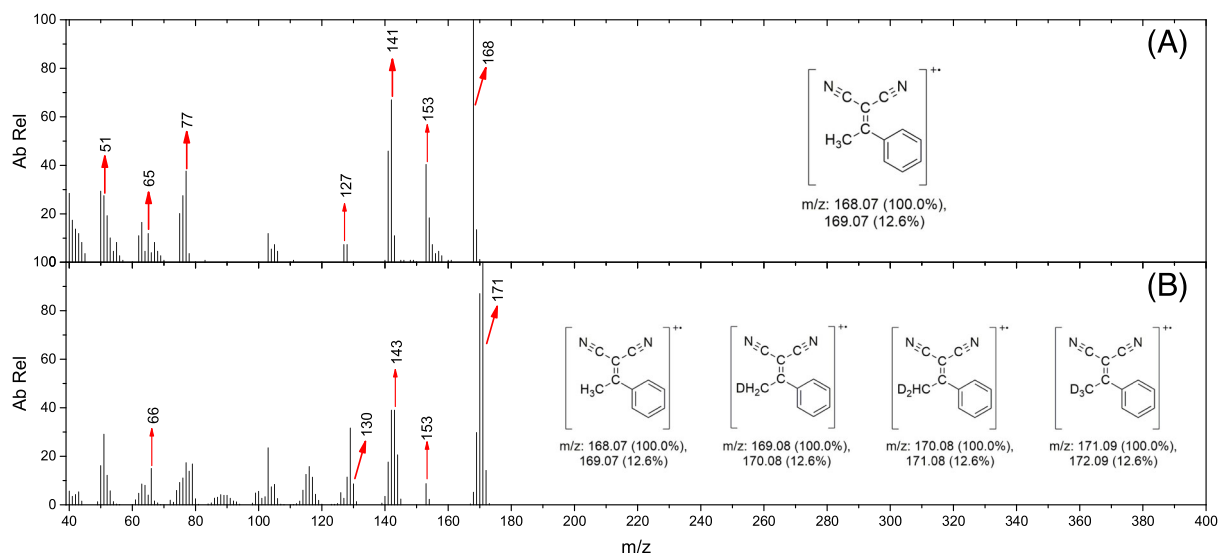


FIGURE 2 Mass spectra of (A) 2-(1-phenylidene) malononitrile and (B) 2-(1-phenylidene) malononitrile-d.

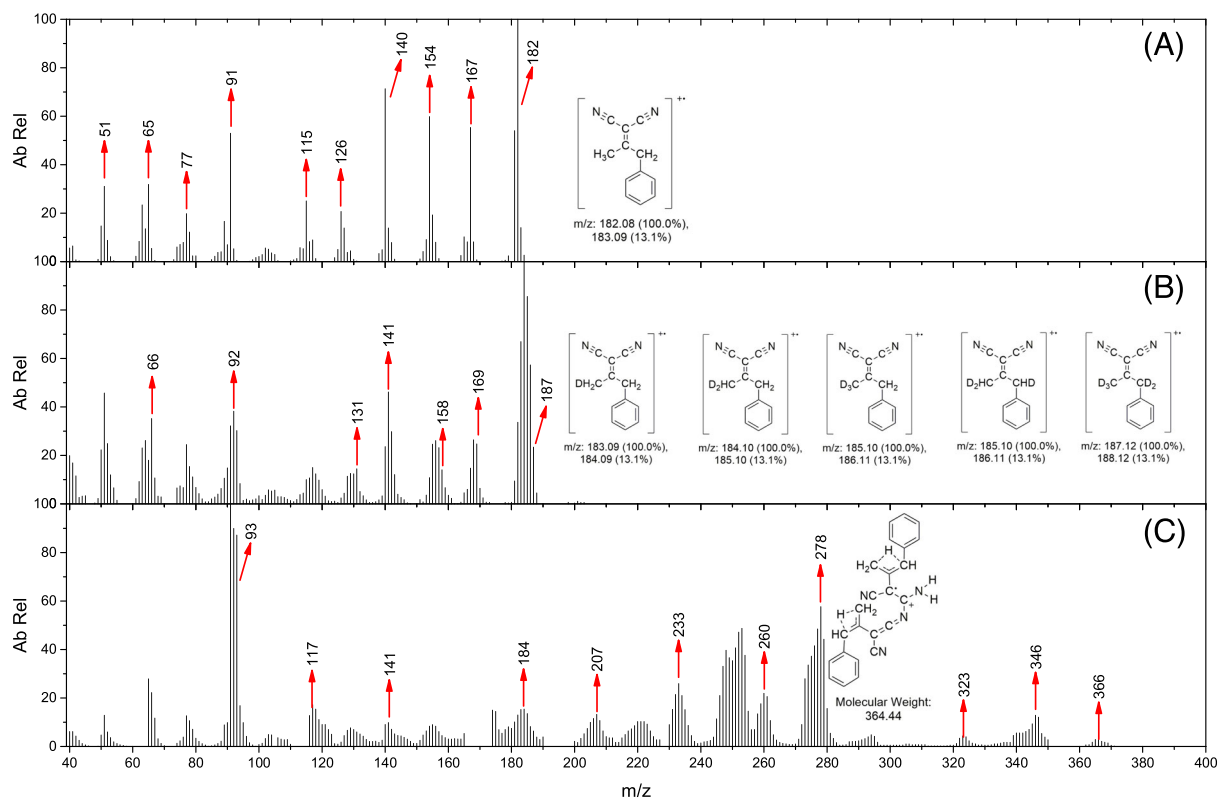


FIGURE 3 Mass spectra of (A) 2-(1-phenylpropan-2-ylidene) malononitrile, (B) 2-(1-phenylpropan-2-ylidene) malononitrile-d and (C) dimeric form.

shows the fragmentation paths that lead to the most important peaks of the BIM MS: m/z 154 (molecular ion), m/z 127, m/z 103, and m/z 76.

Figure 2 illustrates the mass spectrum of FIM. Figure S2 shows the corresponding chromatogram, and Scheme 3 shows the fragmentation paths that lead to the

most important peaks of the MS of FIM: m/z 168 (molecular ion), m/z 153, m/z 141, m/z 140, m/z 77, m/z 63, and m/z 51. Interestingly, the peak at m/z 65 could only be justified by a direct cleavage from the tautomeric cetenimine form from the ionized molecular ion in the ketenimino double bond. This inductive cleavage would be

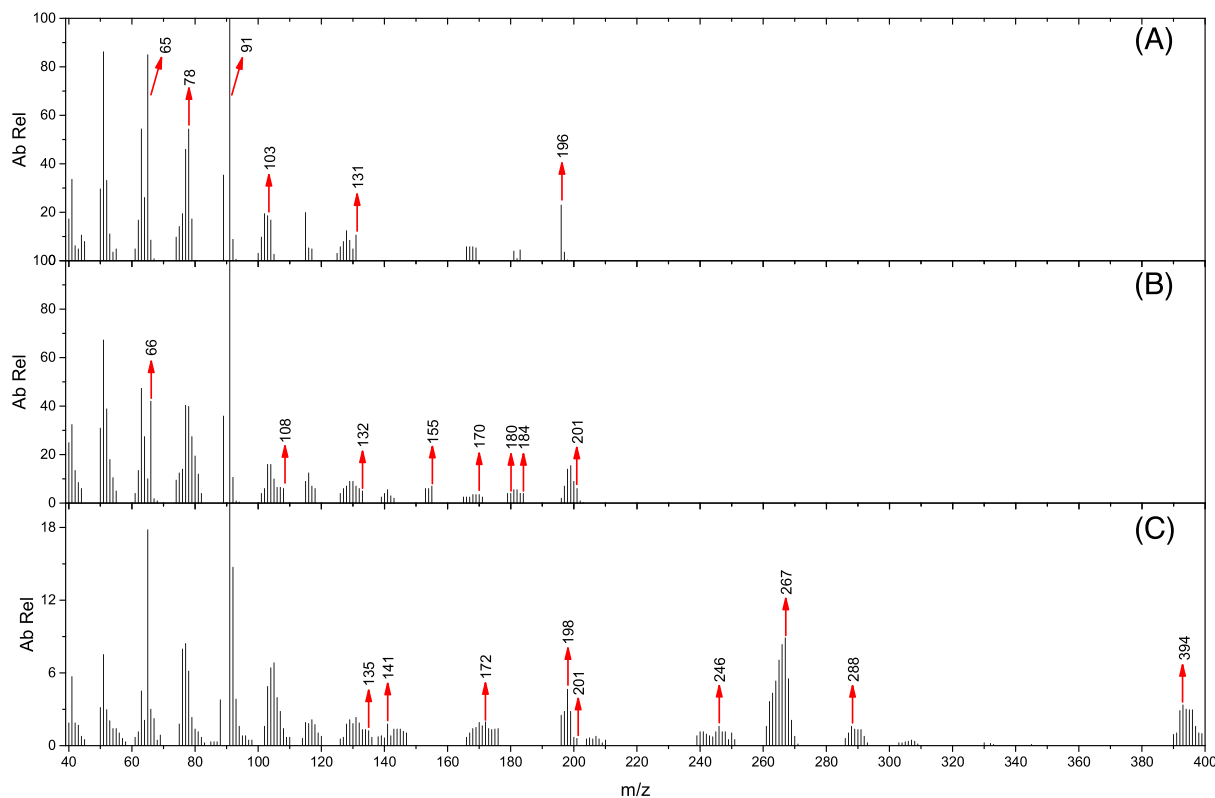
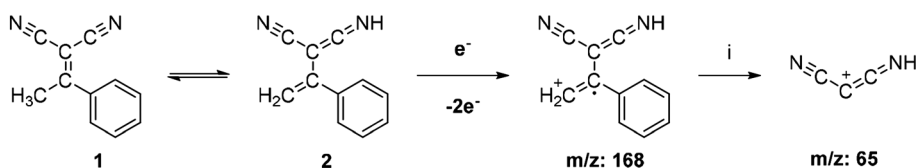


FIGURE 4 Mass spectra of (A) 2-(4-phenylbutan-2-ylidene) malononitrile, (B) 2-(4-phenylbutan-2-ylidene) malononitrile-d and (C) dimeric form.



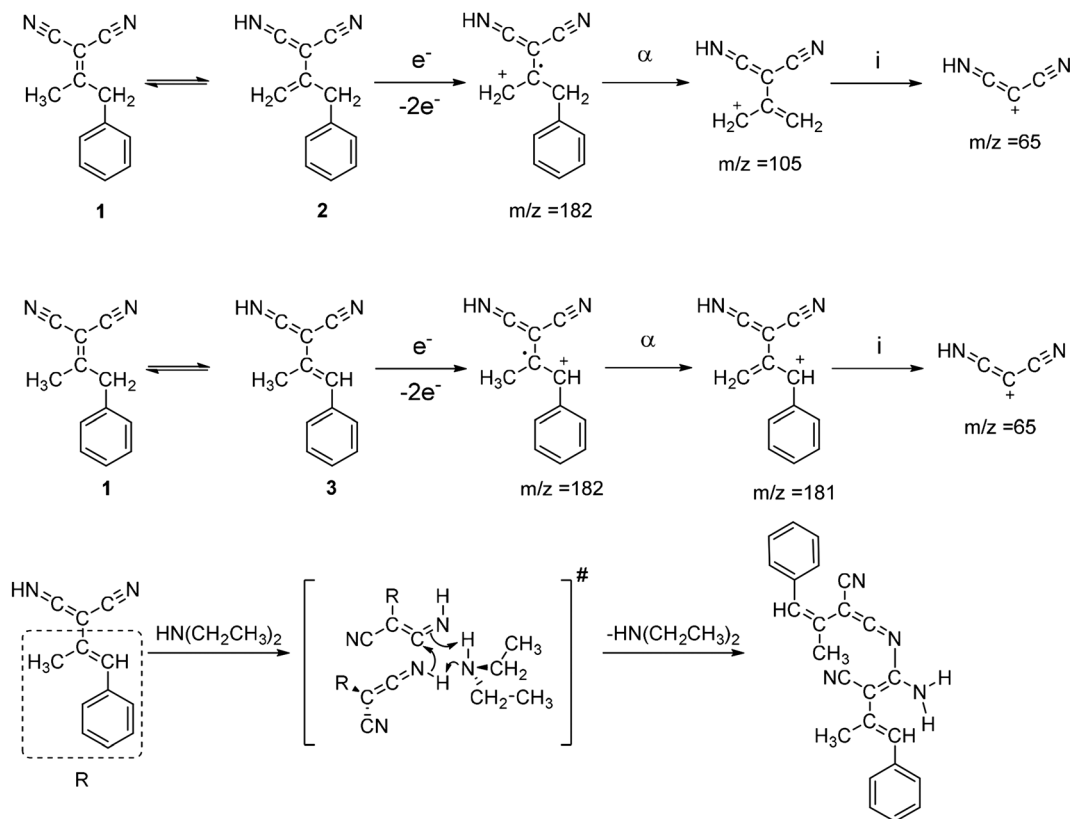
SCHEME 3 Fragmentation path that produces the peak at m/z 65 from the ketenimine tautomer (ketenimine form). (1) Nitrile form and (2) ketenimine form.

explained by the resonance stabilization of the benzyl type radical (Scheme 3).

If the mass spectrum of the nondeuterated FIM is compared with the corresponding deuterated FIM spectrum, the shift to higher masses of certain characteristic peaks can be observed. First, the molecular ion (base peak of both spectra) moves to m/z 171, suggesting an exchange of 3H for D. The peak at m/z 141 moves to m/z 144, indicating that it may have exchanged 3H. On the other hand, the peak at m/z 153, as expected, maintains the m/z value because it results from the loss of methyl from the molecular ion by alpha cleavage (Scheme 3). When analyzing the original peak of the ketenimine form, the abundance ratio of m/z 65 and m/z 66 is reversed from the spectrum of the nondeuterated form to the deuterated form, being m/z 65 more abundant in the undeuterated FIM spectrum and m/z 66 more abundant in the deuterated one.

Figure 3A depicts the mass spectrum of FPIM, Figure S3 shows the corresponding chromatogram, and Scheme 4 shows the fragmentation paths that result in the most important peaks: m/z 182 (molecular ion), m/z 167, m/z 154, m/z 140, m/z 126, m/z 91, m/z 77, and m/z 63. Just like for FIM and as described in Scheme 4, the peak at m/z 65 could only be explained by the tautomeric ketenimine form (form A or B) from the ionized molecular ion in either ketenimino double bond. In this case, unlike in FIM, the fragmentation path begins with an alpha cleavage and then an inductive one.

In the deuterated FPIM spectrum (Figure 3B), peaks shift to higher masses, and peak bands generated around each characteristic m/z can be observed. As expected, unlike FIM, the molecular ion of FPIM (base peak of both spectra) reaches up to m/z 187, suggesting an exchange of up to 5H for D. The ratio m/z 167 moves to m/z 169, m/z 154 to m/z 159, m/z 140 to m/z 141, m/z



SCHEME 4 Fragmentation path that produces the peak at m/z 65 from the ketenimine tautomer (ketenimine form, R or B). Proposed mechanism to produce the 2-(1-phenylpropan-2-ylidene) malononitrile dimer. (1) Nitrile form, (2) ketenimine form A, and (3) ketenimine form B.

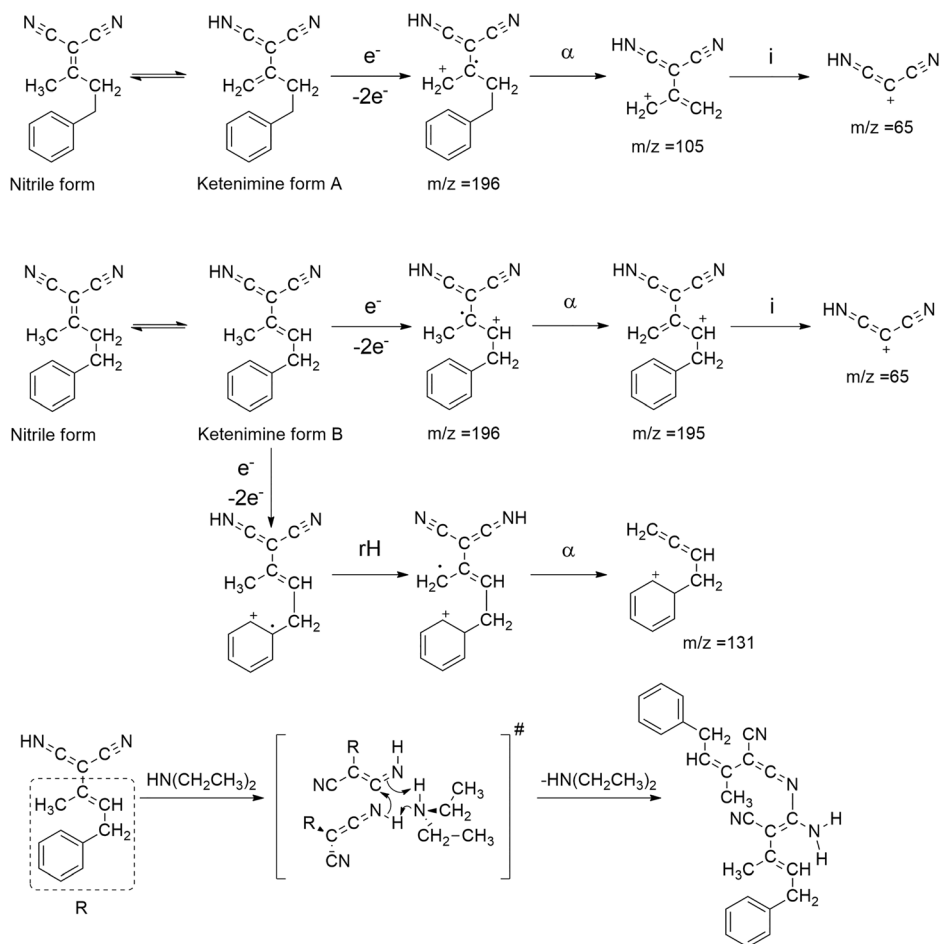
126 to m/z 131, and m/z 91 to m/z 93 (Scheme 4 displays the fragmentation paths). As in the case of FIM, when the original peak of the ketenimine form is analyzed, the abundance ratio of m/z 65 and m/z 66 is reversed from the spectrum of the nondeuterated form to the deuterated one, 65 being more abundant in the undeuterated FPIM spectrum and 66 in the deuterated one.

The FPIM chromatogram, unlike FIM, showed two peaks: One corresponds to the deuterated spice and the other shows a mass spectrum suggesting a dimeric structure. Based on experimental evidence of nitrile–ketenimine tautomerism, Cisneros et al.^{25,26} studied some organic chemistry reactions involving the ketenimine tautomer as a specific reagent. The authors evidenced the dimer formation of unsaturated malononitriles catalyzed by diethylamine, postulating a mechanism which exclusively occurs via the ketenimine tautomer. The proposed mechanism is shown in Scheme 4 for FPIM. The mass spectrum of Figure 3C corresponds to the spectrum of the proposed dimer. Scheme 3 also shows the fragmentation paths that result in the most important peaks of the spectrum of the proposed dimer.

Figure 4A depicts the mass spectrum of FBIM. Figure S4 illustrates the corresponding chromatograms,

and Scheme 4 shows the fragmentation paths that produce the most important peaks: m/z 196 (molecular ion), m/z 104, m/z 91 (base peak), m/z 78, and m/z 63. Like FIM and FPIM and as shown in Scheme 5, the peak at m/z 65 could only be justified by tautomeric ketenimine forms (form A or B) from the ionized molecular ion in either ketenimino double bond. In these cases, the fragmentation path begins with an alpha cleavage and then an inductive one. The peak at m/z 131 is justified only by the form of ketenimine B, after a rearrangement of H and an alpha cleavage, starting from the ionized compound on the aromatic ring (Scheme 5).

In the deuterated FBIM spectrum (Figure 4B), most peaks shift to higher masses, and peak bands generated around each characteristic m/z can be observed. In the case of FBIM, as it was also observed for FPIM, the molecular ion moves up to m/z 201, suggesting an exchange of up to 5H for D. The ratio m/z 167 moves to m/z 169, m/z 154 to m/z 159, m/z 140 to m/z 141, m/z 126 to m/z 131, and m/z 91 to m/z 93 (Scheme 5 presents the fragmentation paths). As in the case of FIM, when analyzing the original peak of the ketenimine form, the abundance ratio of m/z 65 and m/z 66 is reversed from the spectrum of the nondeuterated form to the deuterated



SCHEME 5 Fragmentation path that produces the peak at m/z 65 and m/z 131 from the ketenimine tautomer (ketenimine form, R or B). Proposed mechanism to produce 2-(4-phenylbutan-2-ylidene) malononitrile dimer. (1) Nitrile form, (2) ketenimine form A, and (3) ketenimine form B.

one, 65 being more abundant in the undeuterated FPIM spectrum and 66 in the deuterated one.

FBIM chromatogram, like that of FPIM, presented two peaks: One corresponds to the deuterated spice and the other shows a mass spectrum suggesting a dimeric structure. Figure 4C illustrates the mass spectrum of the corresponding dimer, and Scheme 5 shows the mechanism of dimer formation as postulated by Cisneros et al.^{25,26} Scheme 5, in turn, presents the fragmentation paths that produce the most important peaks of the spectrum of the proposed dimer.

Table 2 lists the percentages of each actual deuterated form for FIM, FPIM, and FBIM. These values were calculated on the basis of the mass spectra of the deuterated compounds, subtracting the $M + 1$ isotopic contribution of each $M - 1$ peak from its corresponding M peak. As regards FPIM, the contribution from each peak of peak $M - 1$ present in the spectrum was also subtracted.

It is worth noticing that for FIM and FBIM, d_2 and d_3 populations are the most abundant in the mass spectra of the deuterated compounds. As far as FIM is concerned, due to its structure, a maximum of up to 3H can be exchanged for D from the methyl that results in the only possible ketenimine form (Scheme 2). In the case of

TABLE 2 Percentages of each actual deuterated form for FIM, FPIM, and FBIM.

	% d_0	% d_1	% d_2	% d_3	% d_4	% d_5
FIM	2.52	14.11	40.31	43.06		
FPIM	9.58	24.64	33.13	18.54	13.39	0.79
FBIM	4.25	14.24	27.59	28.71	14.71	10.49

Abbreviations: FIM, 2-(1-Phenylidene) malononitrile; FBIM, 2-(4-Phenylbutan-2-ylidene) malononitrile; FPIM, 2-(1-Phenylpropan-2-ylidene) malononitrile.

FBIM, due to its structure, a maximum of 5H can be exchanged for D from the methyl that originates the ketenimine A form and the one that originates the ketenimine B form (Scheme 2). Regarding FPIM, d_2 population is the most abundant in the mass spectra of the deuterated compound, and despite being able to exchange a maximum of up to 5H for D, it is suggested that the d_2 structure results from the methylene that originates the ketenimine B form, due to the great conjugation that this tautomeric form has given its aromatic ring.

As it can be seen in Schemes 3 and 4, the mechanism of dimer formation seems to result from the ketenimine

B form, because the FIM compound does not form the dimer structure and has no ketenimine B form.

In order to correlate the experimental results and support the tendencies and observations obtained, geometry optimization calculations were conducted using the DFT theory with hybrid functional B3LYP and set of bases 6-311 ++ g (d, p) (Figures S5 to S13).^{10,27} We also performed frequency calculations in all cases to obtain the corresponding Gibbs free energy standard values ($G \cdot 298.15 \text{ K}$). The analysis of vibrational frequencies allowed us to corroborate that all optimized structures correspond to a minimum in the potential energy surface. The results are shown in Table 3, and the values show that nitrile form is more stable than the ketenimine form in all cases.

Differences in Gibbs free energy predicted that the most stable tautomer should be formed by proton removal from the methyl group (structures A). Experimentally, it has founded for FBIM, whereas the most stable tautomer for FPIM is formed by proton removal from methylene group. To try understand the discrepancies between the theoretical and experimental results, we

TABLE 3 Gibbs free energy standard values differences between nitrile and ketenimine forms for FIM, FPIM, and FBIM.

	Nitrile	Ket A	Ket B
FPIM	0	22.46	17.55
FBIM	0	23.03	19.12
FIM	0	20.06	—

Abbreviations: FIM, 2-1(Phenylidene) malononitrile; FBIM, 2-(4-Phenylbutan-2-ylidene) malononitrile; FPIM, 2-(1-Phenylpropan-2-ylidene) malononitrile.

performed calculations on nitrile structures with a removed proton, generating anionic species, and we have compared the relative stabilities of these new species.

Figures 5 and 6 illustrate the electrostatic map potentials of electrically neutral FPIM and FBIM (A) and the anionic structures generated by the abstraction of an alpha proton from the double bond (B and C).

Coloration allows to distinguish how the electron density is distributed in the molecule. Blue color indicates positive density and red negative density. In the neutral structure of FBIM (Figure 6A), small negative density is housed in the nitrogens, the rest presenting rather neutral density, evidenced by the light blue color. The abstraction of an acidic proton to generate an anion generates density that, despite being housed over the entire molecule, if abstracted from the methyl, presents an electronic distribution that reaches the aromatic nucleus with more intensity (comparison of Figure 6B,C). This fact gives more stability to the anion generated by the hydrogen abstraction from the methyl rather than from the methylene.

As for FPIM, with respect to FBIM, a more delocalized negative density can be seen in the neutral entity (Figure 5A) in every molecule, also a more greenish coloration, owing to the proximity of the aromatic nucleus to the densely negative group that contains the nitrogen.

As regards the formation of an anion by abstracting an alpha proton from the double bond, a great density of negative charge distributed over the entire molecule can be observed when the abstraction is from methylene. In turn, when the abstraction of a hydrogen is from methyl, the degree of intensity is not such. Conjugation with the aromatic nucleus provides additional stability to the anion in Figure 5B as compared with Figure 5C.

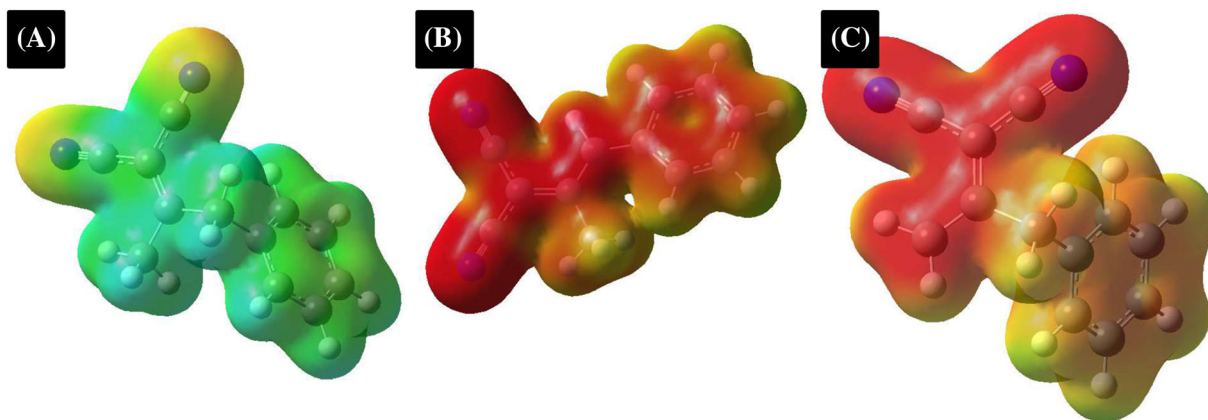


FIGURE 5 Electrostatic potential maps of (A) electrically neutral FPIM; (B) anionic FPIM generated by the abstraction of a methylenic H; and (C) anionic FPIM generated by the abstraction of a methylic H. The results of the relative energies show a more stable structure B than structure C by 7.02 Kcal/mol. Gray represent carbons, blue represent nitrogen, and white represent hydrogens. FPIM, 2-(1-Phenylpropan-2-ylidene) malononitrile.

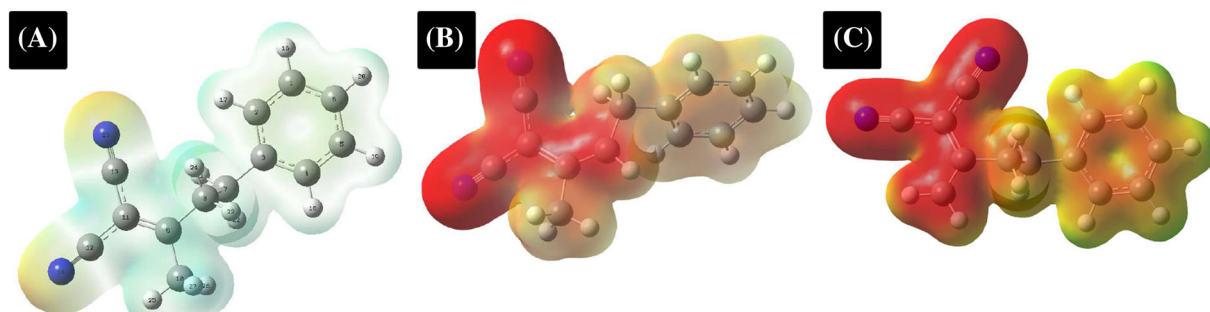


FIGURE 6 Electrostatic potential maps of (A) electrically neutral FBIM; (B) anionic FBIM generated by the abstraction of a methylenic H; and (C) anionic FPIM generated by the abstraction of a methylic H. The results of the relative energies reveal a more stable structure C than structure B by 2.10 Kcal/mol. Gray represent carbons, blue represent nitrogen, and white represent hydrogens. FBIM, 2-(4-Phenylbutan-2-ylidene) malononitrile.

According to the observations, the most favored tautomer in the case of FBIM seems to be the one formed by the removal of a proton from the methyl group. On the other hand, regarding FPIM, the most favored tautomer is the one that forms toward the methylene side, which is expected given the great stabilization offered by its aromatic center. These results are in agreement with the contributions of each deuterated form obtained from the mass spectra on FPIM and FBIM. For FBIM, d_2 and d_3 populations are the most abundant in the mass spectra of the deuterated compound. Said populations would derive from the ketenimine A form, the most stable structure based on the geometric optimization calculations. On the contrary, regarding FPIM, d_2 population is the most abundant in the mass spectra of the deuterated compound. Said population would derive from the ketenimine B form, the most stable structure according to the geometric optimization calculations, and in line with the great resonance stabilization obtained by its proximity to the aromatic ring.

4 | CONCLUSIONS

The nitrile–ketenimine equilibrium has been successfully studied in a family of new unsaturated malononitriles. This type of equilibrium, not yet thoroughly explored for this class of compounds, has been examined using isotopic exchange experiments with mass spectrometry and DFT theory with the hybrid functional B3LYP 6-311 ++ (d, p).

Our results evidenced that the degree of deuteration is strongly related to the chemical structure of the unsaturated malononitriles analyzed, showing a clear dependence on the prevalent ketenimine form. The substituents have been strategically varied in order to determine the role they play in the displacement of the equilibrium studied.

Methyl and methylene tautomeric structures were approached and a greater displacement toward the tautomeric methyl form in the case of no additional conjugation toward an aromatic ring was established. In the case of a methylene structure conjugated with an aromatic ring, our results, both experimental and theoretical, suggest a greater shift toward this more stable tautomeric methylene form.

Finally, the structures with a potential tautomeric methylene ketenimine form produced dimeric structures, regardless of whether the tautomeric methylene form was stabilized or not, by conjugation with an aromatic ring, as mentioned above.

This work sheds light on the synthesis and structural study of a class of biochemically relevant compounds and helps to understand the influence of different substituents on the nitrile–ketenimine equilibrium displacement. In this way, the report of the parameters that govern the different structural forms of a selected compound can contribute to the development of new potential compounds to be used for different purposes.

ORCID

Juan M. Giussi  <https://orcid.org/0000-0001-9113-9873>

REFERENCES

- [1] S. A. Benner, *Science* **2004**, 306, 625.
- [2] M. Tang, H. Gu, S. He, S. Rajkumar, X. Yang, *Am. Ethnol.* **2021**, 133, 21504.
- [3] S. Masuda, K. Minagawa, *Prog. Polym. Sci.* **1996**, 21, 557.
- [4] Z. Osifová, R. Reiberger, I. Císařová, A. Machara, M. Dračinský, *J. Org. Chem.* **2022**, 87, 10309.
- [5] J. M. Giussi, B. Gastaca, M. J. Lavecchia, M. Schiavoni, M. S. Cortixo, P. E. Allegretti, *J. Mol. Struct.* **2015**, 1081, 375.
- [6] V. Singh, B. I. Fedeles, J. M. Essigmann, *RNA* **2014**, 21, 1.
- [7] D. Li, B. I. Fedeles, V. Singh, C. Sam Peng, K. J. Silvestre, A. K. Simi, J. H. Simpson, A. Tokmakoff, J. M. Essigmann, *PNAS* **2014**, E3252.

- [8] P. Chatterjee, S. Sankar Dutta, T. Chakraborty, *J. Phys. Chem. A* **2022**, *126*, 1591.
- [9] E. Largy, A. König, A. Ghosh, D. Ghosh, S. Benabou, R. Rosu, V. Gabelica, *Chem. Rev.* **2022**, *122*, 7720.
- [10] D. Ruiz, J. M. Giussi, A. Albeza, M. Schiavoni, J. J. P. Furlong, P. Allegretti, *Spectrochim. Acta, Part A* **2010**, *77*, 485.
- [11] J. M. Giussi, B. Gastaca, A. Albesa, M. S. Cortizo, P. E. Allegretti, *Spectrochim. Acta, Part A* **2011**, *78*, 858.
- [12] F. A. Carey, R. Sundbrg, *J. Adv. Org. Chem. Part B. React. Synth.* **2007**, 147.
- [13] M. H. Elnagdi, M. R. Elmoghayar, E. H. Galal, *Synthesis* **1984**, 1984, 1.
- [14] R. Hegenauro, *Chemotaxonomie der Pflanzen*, Birkhäuser Basel **1962** 1.
- [15] A. Piasecka, N. Jedrzejczak-Rey, P. Bednarek, *New Phytol.* **2015**, *205*, 948.
- [16] J. N. Andexer, N. Staunig, T. Eggert, C. Kratky, M. Pohl, K. Gruber, *ChemBioChem* **1932**, *2012*, 13.
- [17] N. E. Kayaleh, R. C. Gupta, F. Johnson, *The Journal of Organic Chemistry* **2000**, *65*, 4515.
- [18] C. L. Stevens, R. C. Freeman, K. Noll, *J. Org. Chem.* **1965**, *30*, 1718.
- [19] S. Trofimenko, E. L. Little Jr., H. F. Mower, *J. Org. Chem.* **1962**, *27*, 433.
- [20] C. L. Stevens, J. C. French, *J. Am. Chem. Soc.* **1953**, *75*, 657.
- [21] K. Sung, S. H. Wu, S. Y. Sun, *J. Org. Chem.* **2002**, *67*, 4298.
- [22] Y. Tomioka, K. Ohkubo, H. Maruoka, *J. Heterocycl. Chem.* **2007**, *44*, 419.
- [23] M. Costa, F. Areias, L. Abrunhosa, A. Venâncio, F. Proença, *J. Org. Chem.* **2008**, *73*, 1954.
- [24] Z. P. Hu, C. L. Lou, J. J. Wang, C. X. Chen, M. Yan, *J. Org. Chem.* **2011**, *76*, 3797.
- [25] H. Saraví Cisneros, S. Laurella, D. L. Ruiz, A. Ponzinibbio, P. E. Allegretti, J. J. P. Furlong, *Int. J. Spectrosc.* **2009**, 408345.
- [26] H. Saraví Cisneros, M. F. Erben, C. O. Della Vedoba, S. Laurella, P. E. Allegretti, J. J. P. Furlong, *Eur. J. Mass Spectrom.* **2011**, *17*, 125.
- [27] M. K. Shukla, J. Leszczynski, *WIREs Comput. Mol. Sci.* **2013**, *3*, 637.

SUPPORTING INFORMATION

Additional supporting information can be found online in the Supporting Information section at the end of this article.

How to cite this article: F. M. Garófalo, B. Gastaca, A. Albesa, J. J. P. Furlong, P. E. Allegretti, J. M. Giussi, *J Phys Org Chem* **2023**, *36*(8), e4511. <https://doi.org/10.1002/poc.4511>